New insights into chlorophyll-WSCP (water-soluble chlorophyll proteins) interactions : The case study of BnD22 (Brassica napus drought-induced 22 kDa)

Youssef Bouargalne, Céline Raguénès-Nicol, Florian Guilbaud, Angélique Cheron, Vanessa Clouet, Carole Deleu, Françoise Le Cahérec

New insights into chlorophyll-WSCP (water-soluble chlorophyll binding proteins) interactions the case study of BnD22 (*Brassica napus* drought-induced 22 kDa)

Bouargalne Youssef[1], Raguénès-Nicol Céline[2], Guilbaud Florian[1], Cheron Angélique[3], Clouet Vanessa[1], Deleu Carole[1] and Le Cahérec Françoise[1]

Author affiliations

1. Univ Rennes 1, INRAE, Institut Agro, IGEPP - UMR 1349, 35653, Le Rheu, France.
2. Univ Rennes 1, INSERM, EHESP, Irset - UMR 1085, 35043 Rennes, France.
3. Univ Rennes1, CNRS, IGDR - UMR 6290, 35000 Rennes, France.

Corresponding author

*Le Cahérec Françoise

UMR 1349 IGEPP (Institut de génétique et protection des plantes), INRAE, Institut Agro, Université de Rennes 1, BP 35327, 35650 Le Rheu, France

francoise.le-caherec@univ-rennes1.fr

Author Contributions

L.C.F. and C.D. acquired financial support, conceived, designed and supervised the research. Y.B. conceived, designed and performed experiments, analyzed data, prepared figures and wrote the original draft. V.C. and A.C, prepared expression plasmids and contributed to protein purification. F.G. performed the protein purification and EMSA experiment. C.R.N. conceived, designed, validated and performed technical guidance for the MST experiments. All authors have read and agreed to the published version of the manuscript.

Abstract

The water-soluble chlorophyll-binding proteins (WSCP) of class II from *Brassicaceae* are non-photosynthetic proteins that bind chlorophylls (Chls) and chlorophyll derivatives. Their physiologic functions, biochemical roles and mode of action are still unclear. It is assumed that the WSCPs have a protection function against Chl photodamage during stressful conditions. WSCPs are subdivided into class IIA and class IIB according to their apparent Chla/b binding ratio. Although their Chla/Chlb binding selectivity has been partly characterized, their Chl affinities are not yet precisely defined. For instance, WSCPs IIA do not show any Chl binding preference while WSCPs IIB have greater affinity to Chlb. In this study, we present a novel method for assessment of Chl binding to WSCPs based on the differences of photobleaching rates in a large range of Chl/protein ratios. The protein we have chosen to study WSCP is BnD22, a WSCP IIA induced in the leaves of *Brassica napus* under water deficit. BnD22 formed oligomeric complexes upon binding to Chla and/or Chlb allowing a protective effect against photodamage. The binding constants indicate that BnD22 binds with high affinity the Chls with a strong selectivity to Chla. Moreover, dependently of Chl/protein ratio, two distinct binding events were detected resulting from difference of Chl stoichiometry inside oligomeric complexes.

Keywords: Chl binding constants,; photobleaching, microscale thermophoresis

Abbreviations:

At: *Arabidopsis thaliana*; BnD22: *Brassica napus* drought-induced 22 kDa protein; Bo: *Brassica oleracea*; BR: bleaching rate; Chl: chlorophyll; DDM: n-dodecyl β-D-maltoside; EC50: half-maximal effective concentration; EMSA: electrophoretic mobility shift assay; ER : endoplasmic reticulum; IF: initial fluorescence; IGEPAL: octyl phenoxy poly(ethyleneoxy)ethanol branched; IPTG: isopropyl β-D-1-thiogalactopyranoside; Kd: dissociation constant; LED: light emitting diode; Lv: *Lepidium virginicum;* MST: microscale thermophoresis; nHill: Hill coefficient; NP40: nonidet P40 substitute; OG: octyl β-D-glucopyranoside; PAGE: polyacrylamide gel electrophoresis; SDS: Sodium dodecyl sulfate; UV: ultraviolet; WSCP: water soluble chlorophyll binding proteins.

1. Introduction

Class II water-soluble chlorophyll proteins (WSCP), specific to *Brassicaceae*, strikingly differ from other Chl-binding proteins. They are water soluble, contain no carotenoid and are not involved in photosynthesis. Class II WSCPs can be categorized into two sub-classes: the class IIA with Chla/b ratio higher than 6 and the class IIB with Chla/b ratio lower than 3.5 (Satoh *et al.*, 2001; Prabahar *et al.*, 2020). Although their biological function and mode of action remain unclear, it is assumed they have a protective function throughout environmental constraints. For example, some of them are induced under stressful abiotic conditions (Downing *et al.*, 1992; Reviron *et al.*, 1992; Annamalai and Yanagihara, 1999; Desclos *et al.*, 2008). Furthermore, it was shown that AtWSCP from *Arabidopsis thaliana* was involved in defenses against herbivores and played a role in programmed cell death during flower development (Boex-Fontvieille *et al.*, 2015a, b). As members of Kunitz-type protease inhibitors, WSCPs have potential function of inhibition against serine and/or cysteine proteases. Thus, AtWSCP and BnD22 (*Brassica napus* drought-induced 22 kDa) are able to inhibit cysteine and serine proteases respectively (Halls *et al.*, 2006; Desclos *et al.*, 2008; Boex-Fontvieille *et al.*, 2015; Rustgi *et al.*, 2017). However, this ability has never been investigated for the widely studied WSCPs, LvWSCP from *Lepidium virginicum* and BoWSCP from *Brassica oleracea.* Because WSCPs are able to extract Chl from thylakoids, it was proposed that they could play as Chl carriers during reorganization process of photosynthetic apparatus under stress conditions and as Chl scavenger during cell damage (Takahashi *et al.*, 2012, 2013b). Although the Chls bound to WSCP are partially shielded against photodamage, the benefit of Chl-binding to WSCP remains unclear (Damaraju *et al.*, 2011). Surprisingly to date, no WSCP was detected in chloroplast whereas they were found in endoplasmic reticulum (ER) bodies, a special ER-derived compartment that contributes to *Brassicaceae* defense system (Nakano *et al.*, 2014) and in vacuole (Takahashi *et al.*, 2012, 2013b).

Either with Chla and/or Chlb, WSCP form homotetrameric complexes which contain one Chl per apoprotein (Horigome *et al.*, 2007; Palm *et al.*, 2018). Tetrameric complexes are organized into two homodimeric subunits in an open-sandwich conformation in which the Chls molecules are tightly packed in a central hydrophobic cavity (Horigome *et al.*, 2007; Bednarczyk *et al.*, 2016; Palm *et al.*, 2018; Agostini *et al.*, 2019). This arrangement makes WSCP-Chl complexes remarkably stable towards denaturation (Takahashi *et al.*, 2014; Palm *et al.*, 2017). This stability is mainly due to the interactions of the Chl phytyl chains with each other within the tetramer (Agostini *et al.*, 2019; Palm *et al.*, 2019). Stable WSCP-Chl tetramers

are also formed with two Chls instead of four (Theiss *et al.*, 2007; Renger *et al.*, 2011; Palm *et al.*, 2017). Although proteins of the class IIA and class IIB are highly homologous in term of structure, the class IIB proteins show a preference to Chlb while proteins of class IIA have no clear preference (Takahashi *et al.*, 2013a, 2013b; Bednarczyk *et al.*, 2015; Palm *et al.*, 2018). This Chla/b specificity involves a loop in close contact to the C_7 side chain of the chlorin macrocycle, where Chla differs structurally from Chlb (Agostini *et al.*, 2019; Palm *et al.*, 2019). Recently, using circular dichroism (CD) spectroscopy-based method, Girr *et al.* (2020) attributed the Chla/b preference to a thermodynamical control and estimated WSCP affinity for Chls.

In this study, we proposed a novel method to quantify and precisely determinate WSCP affinity for Chls from a label free strategy derived from microscale thermophoresis (MST). MST provides a sensitive and reliable method to analyze and to quantify molecule interactions A temperature gradient created by infrared laser (IR) causes a motion of molecules strongly linked to their charge, size and solvation, properties which vary upon their binding. This powerful fluorescence-based technique allows precise measurements of binding affinities range from µM to pM (Wienken *et al.*, 2010; Jerabek-Willemsen *et al.*, 2014). We focused our study on BnD22, the major WSCP IIA expressed in *B. napus* leaves by following Chl-WSCP interactions. *In vivo*, this protein undergoes a post-translational maturation with a cut-off in the C-terminal region, without effect on its biological properties (Ilami *et al.*, 1997; Takahashi *et al.*, 2014). Using His tagged-BnD22 without its C-terminal region, bindings with Chla and/or Chlb were monitored qualitatively by EMSA (electrophoretic mobility shift assay) coupled with absorption spectra. The binding constants were determined with a MST-derived approach based on the photobleaching rates observed during excitation, before IR application, dependently on Chl/protein ratios. We show that i) BnD22-Chl complexes protect the Chls against photodamage, ii) depending on Chl/apoprotein ratio, two distinct binding events are detected for both Chla and Chlb, each with a specific binding affinity, iii) the two distinct binding events reflect a different Chl stoichiometry inside oligomeric complexes and iv) BnD22 binds preferentially Chla compared to Chlb.

2. Material and methods

2.1. Protein expression and purification

The mature form of BnD22, without peptide signal neither C-terminal extension, was amplified from genomic DNA of *Brassica napus* (Darmor nain accession) using forward and

reverse primers, 5'AATTTTGTTTAACTTTAAGAAGGAGATATACATATGAGAGAACAGGTGAAGGACTC3' and 5'CAGTGGTGGTGGTGGTGGTGAGCAGCATCATCAACTTTCA3' respectively. The amplified sequence was cloned into NcoI-Xhol sites of the pET-21a (+) expression vector (Novagen) using Gibson assembly approach (New England Biolabs). The construct was introduced into *E. coli* Rosetta-gami 2(DE3) (Novagen) to produce recombinant BnD22 carrying a C-terminal hexa-histidine tag (BnD22).

Bacterial cells were grown at 37 °C in 500 mL LB media containing 100 µg.mL^{-1} ampicillin and 10 µg.mL^{-1} tetracycline until the A_{600nm} reached 0.6. Expression of recombinant protein was induced with 1 mM isopropyl β-D-1-thiogalactopyranoside (IPTG) for an additional 4 h of culture. The cells were harvested by centrifugation (5000×g, 15 min, 4°C) and resuspended in lysis buffer containing 50 mM sodium phosphate (pH 8.0) buffer, 300 mM NaCl, 5 mM imidazole, 1 mg.mL^{-1} lysozyme, 3.3 µg.mL^{-1} DNase I and protease inhibitor cocktail (Roch). After sonication, the supernatant and pellet fractions were separated by centrifugation (14000×g, 10 min, 4°C).

Soluble BnD22 was purified from supernatant with Ni^{2+}-chelating affinity chromatography (Protino Ni-NTA column, Macherey-Nagel) according to the manufacturer's instructions. Briefly, the supernatant fraction was loaded onto column previously equilibrated with buffer containing 50 mM sodium phosphate (pH 8.0) buffer, 300 mM NaCl and 5 mM imidazole. The column was washed by increasing the imidazole concentration from 5 to 75 mM and the proteins were eluted with 250 mM imidazole. Purified BnD22 was concentrated and buffer-exchanged against 50 mM Tris-HCl (pH 7.5) buffer, 150 mM NaCl on 10 kDa centrifugal filter unit (Merck Millipore). Protein concentration was determined at 280 nm using extinction coefficient and molecular weight calculated by the online ExPasy ProtParam tool (https://web.expasy.org/protparam/). The bacterial expression profile and the quality of purified recombinant BnD22 were analyzed by SDS-polyacrylamide gel electrophoresis (SDS-PAGE) followed by Coomassie blue staining (Laemmli, 1970). Purified protein was stored at -20 °C until further use.

2.2. Electrophoretic mobility shift assay and UV-visible absorption spectra

BnD22 at 20 µM in 50 mM Tris-HCl (pH 7.5) buffer, 150 mM NaCl, 0.04% Nonidet-P40 (NP40) was mixed with Chla or Chlb (Sigma) solubilized in 100 % ethanol to reach final 5, 10, 15, 20, 40 or 60 µM concentrations (0, 0.25, 0.5, 0.1, 1, 2 or 3 ratio Chls/protein) in a final volume of 100 µL. NP40 was chosen for its suitability for the MST analyses. The mixtures

were incubated in the dark at 4 °C for 30 min and subjected to EMSA using a detergent free 12 % PAGE. Chl fluorescence was detected using a fluorescence imaging system (Fluorcam FC 800-O, Photon System Instruments) and the proteins were visualized by Coomassie blue staining.

For the absorption spectra, BnD22 was reconstituted in excess of Chls. 20 µM of the recombinant protein were mixed with 60 µM of Chla or Chlb or mix of Chla/b at three different Chl/protein ratios (1/1, 3/1, 10/1). After binding step, the mixtures were subjected to 12 % native PAGE and the greenish band corresponding to the reconstituted complexes BnD22-Chls was eluted from gel in 50 mM Tris-HCl (pH 7.5) buffer, 150 mM NaCl. The absorption spectra were measured between 300 and 750 nm using NanoDrop™ One (Thermo Scientific).

2.3. Détermination of Chl/protein stoichiometry

Based on results published by Palm *et al.* (2017), we chosen 5-fold Chl molar excess and 40-fold BnD22 molar excess for two binding conditions, to determine the molar Chl/protein ratio from absorption spectra of purified BnD22-Chla or BnD22-Chlb complexes. Chl concentrations were determined based on extinction coefficients of Chls bound to BnD22 and the absorption values at the Qy absorption maxima. Protein concentration was determined using absorption values at 280 nm taking into account the contributions of Chla or Chlb to the absorption at this wavelength and BnD22 extinction coefficients.

2.4. Development of a method based on use of MST

To follow BnD22/Chl interactions, the intrinsic fluorescence of Chls was monitored to enable a label-free MST analysis. All MST equipment: Monolith NT.115 instrument, Monolith NT^{TM} capillaries (standard or premium) and software (MO.control, NT.control, MO.affinity analysis) used are from NanoTemper technologies GmbH. Measurements were performed at the Spectroscopies-DCTP core facility (UMS Biosit, Université de Rennes 1- Campus de Villejean- 35043 RENNES Cedex, FRANCE).

2.4.1. Buffer selection and optimal ligand concentration range

To determine the optimal buffer composition for Chl stability and homogeneity during measurement, fluorescence capillary scan and MST signals were recorded in several buffers : Tris-buffer (50 mM Tris-HCl (pH 7.5), 150 mM NaCl) or phosphate-buffer (50 mM (pH 7.5), 150 mM NaCl) supplemented with non-ionic detergents : 0.04% NP40, 0.3 % n-dodecyl β-D-maltoside (DDM), 1 % octyl β-D-glucopyranoside (OG) and 20 % octylphenoxy

poly(ethyleneoxy)ethanol (IGEPAL). Chla and Chlb solubilized in 100 % ethanol were diluted in the different buffers at final concentrations of 50 and 80 nM respectively to yield detectable fluorescent signals. The samples were filled into standard capillaries for measurement.

2.4.2. Preparation of reaction mixtures for MST experiments

For the binding assay, a constant concentration of Chla (50 nM) or Chlb (80 nM) was mixed with a serial dilution of non-labeled BnD22 using Tris-buffer with 0.04 % NP40 as binding buffer. The concentrations of BnD22 varied from 80 µM to 0.124 nM (2.44-fold serial dilution) and from 80 µM to 2.24 nM (2-fold serial dilution) with Chla and Chlb respectively. All binding mixtures were incubated for 30 min in the dark at 4°C and filled into standard treated (Chla) or premium (Chlb) capillaries for MST measurements. All experiments were repeated three times with different purification batches of BnD22. As negative controls, trypsin and lysozyme (concentrations from 80 µM to 2.24 nM), non-binding and unrelated Chl proteins, were used instead of the recombinant BnD22 protein.

2.4.3. MST measurements, data acquisition and analysis

All MST measurements were conducted on a Monolith.NT115 instrument, at 100 % LED (light emitting diode) power and 40 % MST power. The data for Chla experiments were acquired with MO.control v2.3 software using nano-red fluorescence channel with laser off/on times of 5.5 and 6 s respectively. For Chlb MST experiments, NT.control v2.1.31 software with blue-red fluorescence channel with 20 s/ 5s laser off/on times was used (Fig. S1). The most appropriate wavelength for excitation/emission of Chls fluorescence in the Monolith.NT115 instrument was beforehand determined by fluorescence emission spectra after excitation at 470 nm or 625 nm (Fig. S1). The maximum emission wavelengths of Chla and Chlb (λ_{max} 675 and 657 nm respectively) are compatible with Monolith NT.115 red detector.

The photobleaching observed during excitation (100% LED) has been used for analyses. Ligand-induced photobleaching rates on the first 5 s of MST traces were calculated using the expert mode bleaching rate in the MO.affinity analysis software to derive binding affinities. The bleaching rates were normalized to response amplitude by equation 1, and plotted against the concentration of the BnD22. To determine the dissociation constant (Kd), the data were fitted to the Kd binding model (equation 2) which describes a reversible molecular interaction with a 1:1 stoichiometry according to the law of mass action. The half-maximal effective concentration (EC50) and cooperativity Hill coefficient (nHill) were obtained from fitting the data with the Hill equation (equation 3).

Equation 1:

$$\text{response amplitude} = 1 - \left[\frac{\text{value (C)} - \text{max value}}{\text{min value} - \text{max value}} \right]$$

where value (C) is the photobleaching value measured for the concentration C, max value is the photobleaching value for the unbound state (lowest BnD22 concentration) and min value is the photobleaching value for the fully bound state (highest BnD22 concentration).

Equation 2:

$$f(C) = \text{unbound} + \frac{(\text{bound} - \text{unbound}) \times (C + C_{target} + Kd - \sqrt{(C + C_{target} + Kd)^2 - 4 \times C \times C_{target}}}{2 \times C_{target}}$$

Equation 3:

$$f(C) = \text{unbound} + \frac{\text{bound} - \text{unbound}}{1 + \left[\frac{EC50}{C} \right]^{nHill}}$$

where f(C) is the response amplitude at a given BnD22 concentration; unbound is the response amplitude of free Chl; bound is the response amplitude of the BnD22-Chl complex; Ctarget is the final concentration of Chl in the assay.

3. Results

3.1. *P*urification of recombinant BnD22 expressed in *E. coli*

Recombinant mature form of BnD22, fused to a hexahistidine (His-tag) in C-terminal, was produced in *E. coli* under IPTG induction (Fig. 1). The produced 20 kDa protein was mainly soluble (about 60 %). A high level of purified recombinant protein was obtained from the soluble fraction through nickel affinity chromatography, with more than 97 % purity assessed by densitometric analysis (Fig. 1). A final large yield of 40 mg per liter of bacterial culture medium was obtained and purified BnD22 was concentrated to 2 $mg.mL^{-1}$ (~0.1 mM) and be kept at -20 °C for long-term storage.

3.2. Qualitative assessment of BnD22 binding to Chls

Binding experiments using different concentrations of Chla or Chlb were performed according to previously methods in presence of a nonionic detergent NP40 instead of methanol (Takahashi *et al.*, 2012), ethanol (Palm *et al.*, 2017) or Triton-X114 (Palm *et al.*, 2018). In our

study, the nonidet P40 was chosen during the binding conditions, for i) its suitability for the MST analyses to provide an adequate level of fluorescence with low amounts of Chla or Chlb (Table 1), ii) its intrinsic properties : a low critical micelle concentration (0,06 mM against 0.2 mM for Triton X114) to minimize the detergent concentration used for Chl solubility, a cloud point of 45-50°C (23°C for Triton X114) to avoid heterogeneity of samples with the formation of two phases.

Subsequently, the formation of BnD22-Chl complexes was visualized by EMSA (Fig. 2). The purified monomeric BnD22 was produced under an active form as confirmed by its ability to bind Chls. Dependently on the concentration of Chl, the binding induces a structural change with the formation of Chl-binding oligomeric complexes. When BnD22 was incubated at least with an equimolar level of Chla or Chlb, almost all the BnD22 formed oligomers, presumably on a tetrameric state. A minor additional supra-oligomeric complex was also detected. All oligomeric complexes emitted fluorescence refuting the possibility that oligomerization may result artificially from aggregates of BnD22 without Chl. Moreover, no difference in the behaviors of BnD22 reconstituted with Chla or Chlb was detected. This result might support the idea that BnD22 would not have Chl preference for either Chla or Chlb in our binding conditions. This was confirmed by absorption spectrum data (Fig. 3). The absorption spectra of BnD22 reconstituted with equal or 3 molar ratios of Chla/b (Fig. 3C, D) were a mix of the spectra of BnD22 reconstituted with Chla or Chlb only (Fig. 3A, B). This indicates that BnD22 would bind simultaneously both Chla and b. When the reconstitution was performed with a tenfold excess of Chla compared to Chlb, the absorption spectrum was almost identical to that of BnD22 reconstituted with Chla only (Fig. 3A, E). These spectra analyses suggest that there is no clear preferential binding of BnD22 to Chla or to Chlb.

3.3. Determination of the binding constant for BnD22-Chls

To assess the binding specificity of WSCPs to Chla or Chlb, interactions were investigated through a Monolith.NT115 instrument using the intrinsic fluorescence of Chls. The difficulty was to define buffer conditions to follow the binding between the hydrophobic molecule target (Chl) and the soluble BnD22 protein ligand.

3.3.1. Conditions for Chl fluorescence detection

The supplementation of buffers with detergent is essential to solubilize Chls and prevent their aggregations in aqueous solution. Two buffers Tris-HCl or sodium phosphate, supplemented with several non-ionic detergents (NP40, DDM, OG, IGEPAL) were tested in

presence of a constant concentration of Chla or Chlb (Table 1). None of these binding buffers led to Chl aggregation or Chl adsorption to the capillary walls (data not shown). Whatever buffer nature, the chosen concentrations of Chla at 50 nM or Chlb at 80 nM allow an adequate fluorescence signal (IF) around 240 counts for Chla and 184 counts for Chlb consistent with the recommendations of Monolith NT.115 manufacturer (Table 1). IF was significantly influenced by nature of the detergent and thus NP40 and OG were the more appropriated detergents to allow highest IF. During excitation, a Chl bleaching was observed. The bleaching rates (BR) were more deeply for Chlb (25-32 ‰.s^{-1}) than for Chla (8-12 ‰.s^{-1}). As IF, bleaching was also significantly influenced by nature of the detergent and, in our hands, could not be prevented. Our choice of binding buffer focused on the Tris buffer with NP40 for which the IF/BR ratio was the highest and because it requires a low concentration to allow micelle formation.

3.3.2. Biphasic behavior of BnD22-Chl interaction

Serial dilutions of BnD22 were incubated with constant concentration of Chla and/or Chlb in Tris buffer supplemented with NP40. After loading in capillaries, cap scans showed little variations in IF (less than 10 %), attesting the absence of ligand-dependent fluorescence enhancement or quenching effects (Fig. S2A, B). Furthermore, for both Chls, capillaries profiles showed gaussian distributed fluorescence peaks attesting absence of sticking or adsorption effects (Fig. S2C, D). MST traces were smooth without bumpiness indicating absence of aggregated molecules and good samples quality (Fig. 4).

As observed with Chls alone (Table 1), a Chl photobleaching was also detected in presence of BnD22 and was dependent on BnD22 concentrations (Fig. 4A, B). A photobleaching was also observed in presence of non-relevant proteins as trypsin or lysozyme, used as negative controls, but was not modified by their concentrations (Fig. 4B, D). High quantity of BnD22 reduced strongly the photobleaching from 9.2 to 1.8 ‰.s^{-1} for Chla, and from 27.2 ‰.s^{-1} (34 ‰.s^{-1} for non-relevant proteins) to 8.6 ‰.s^{-1} for Chlb (Fig. 5). This argues in favor of a protective effect of the BnD22-Chl binding against Chl photodamage. Moreover, it appeared that BnD22 protection was significantly higher for Chla (80.3±0.3 %) as Chlb (68.3±0.8 %) (Table 2).

As the BnD22-dependent Chl photobleaching led to strong fluorescence variations, it prevented classical MST temperature-jump analysis. The binding parameters were so determined from the photobleaching rates, according to the recommendations of Monolith NT115 manufacturer. Response amplitude of Chls, calculated from photobleaching rates, were

plotted against BnD22 concentrations (Fig. 6) and used to assess the binding constants of BnD22 to Chla or Chlb (Table 3). For both Chls, typical bi-phasic binding curves were obtained indicating that two binding events have occurred, each with a defined BnD22-Chls affinity. The first event (event 1) was occurred when the quantity of Chla or Chlb was in excess over the protein (low BnD22 concentrations), while the second bining event (event 2) occurred when Chl quantity was limited over protein (high BnD22 concentrations). For event 1, only estimated Kd values could be determined, in the nM range. Anyway, it was possible to discriminate bindings between BnD22-Chla and BnD22-Chlb, 3.9±2.2 nM for Chla and 51.4±8.6 nM for Chlb, suggesting that BnD22 could preferentially bind the Chla (Table 3). This affinity of BnD22 to Chla, around 10 times more than Chlb, was also supported by EC50 values. Bindings at the event 2 were characterized by affinities in order of µM, 1000-fold weaker than those of the event 1. The accurate Kd values of 2.0±0.2 and 6.7±0.7 µM for Chla and Chlb respectively were in the same range than the EC50 values. These values revealed a higher affinity (3-fold) of BnD22 for Chla than for Chlb. For both events, the Hill coefficients were around 1 indicating that the binding would be non-cooperative (Table 3).

According to Palm *et al.* (2017), the stoichiometry of Chl/protein inside complexes was determined (Fig. 6). When BnD22 was reconstituted with a 5-fold molar excess of Chla or Chlb (event 1), the Chl/protein ratio calculated was 1.11±0.02 and 0.88±0.02 respectively reflecting a binding stoichiometry of four Chl per tetrameric complex. When a 40-fold molar excess of BnD22 over Chls was used (event 2), the presence of only two Chls inside complexwas outlined with Chl/protein ratio values of 0,48±0,05 for Chla complexes and 0,43±0,07 for Chb complexes.

4. Discussion

In this study, WSCP-Chl interactions were monitored qualitatively by EMSA coupled with absorption spectra and quantified by decrease in photobleaching with a MST device. We focused on BnD22 protein which belongs to the class of WSCP IIA protein. Recombinant mature BnD22 protein with histidine-tag in C-terminal was expressed in *E. coli*. As well established for numerous other WSCPs, the bacterial expression systems allowed high yields and high purity of recombinant target (Schmidt *et al.*, 2003; Theiss *et al.*, 2007; Takahashi *et al.*, 2012, 2014).

4.1. BnD22 binds both Chla and Chlb

To our knowledge, this is the first report that demonstrates the ability of BnD22 to bind Chls.-. For this purpose, we used recombinant His-tagged BnD22 mature protein since it was shown by several authors that such recombinant protein are appropriate for study WSCPs for their Chl interaction (Schmidt *et al.*, 2003; Theiss *et al.*, 2007; Takahashi *et al.*, 2012, 2013, 2014). EMSA experiments and UV-visible absorption spectra, revealed that BnD22 formed oligomer upon binding to Chla and/or Chlb. However, as shown for BoWSCPs, another WSCP IIA, no clear difference between Chla or Chlb in the binding behavior was detected by this method (Takahashi *et al.*, 2012; Bednarczyk *et al.*, 2015; Palm *et al.*, 2018). To date, only LvWSCP, a WSCP of class IIB, showed a clear preference for Chlb compared to Chla (Takahashi *et al.*, 2013; Palm *et al.*, 2018).

4.2. MST derived method is a tool to characterize Chl-protein binding constants

To get more information about the Chla/Chlb selectivity, we have established a label free MST derived strategy to obtain direct binding constants between water-soluble BnD22 with highly hydrophobic Chls. MST approach has been successful in determining the binding constants for hydrophobic Chl-binding proteins as the light harvesting proteins (Mork-Jansson and Eichacker, 2018, 2019), but has never been used on WSCPs. Establishment of experimental conditions for introducing hydrophobic Chls into an aqueous protein environment compatible for MST measurement was challenging. In previous WSCP/Chl binding methods, Chls were provided either in organic solvents or detergents (Takahashi *et al.*, 2012; Palm *et al.*, 2017, 2018).

The presence of detergents is recommended for MST experiments since they may reduce the adsorption of the molecules to glass capillaries walls and the non-specific interactions driving to aggregation (Khavrutskii *et al.*, 2013; Seidel *et al.*, 2013). After comparison of results obtained for several detergents, we chose 0.04% NP40 providing an adequate level of fluorescence for as little as 50 nM Chla and 80 nM Chlb. These Chls concentrations were 20-fold lower than those previously used (~1 µM) in a CD method where the detection limit of the method did not allow the determination of proper Kd values (Girr *et al.*, 2020). The very low concentrations of Chl required for our proposed MST-derived analysis offer a real advantage by allowing accurate determination of dissociation constants for WSCPs-Chls interactions.

4.3. BnD22-Chls interactions depend on Chl/protein ratio

The dose-response curves of BnD22 binding Chls fit as a biphasic process, each phase representing a distinct binding event. Regardless Chl nature, when Chl was preponderant over

proteins, corresponding to event 1, the affinity was very high, in the order of a few nM. These values were very close to the limit of detection 10 nM for the Monolith NT.115 device (Jerabek-Willemsen *et al.*, 2014). To be more accurate, lower Chls concentrations are required (below the estimated Kd) and could only be analyzed with the Monolith NT Pico, an improved sensitivity instrument designed to detect low fluorophores concentrations (Entzian and Schubert, 2016). Under limiting Chl conditions, a second binding event (event 2) occurred with affinity in the order of µM, 1000-fold weaker than the first one.

This biphasic binding process could be explained by different affinities of the binding sites within the oligomeric complex, even if the Hill coefficients determined under our conditions indicate rather a lack of cooperative effect. The both event 1 and event 2 of binding between Chl and BnD22 could result also from a conformational change of the complexes. As reported for all studied WSCPs, the binding to Chls drives the formation of a tetramer complex, presumably the major complex observed in EMSA experiments. The additional supra-oligomeric complex detected could either be due to an hexamer conformational state as supported by Satoh *et al.* (1998) for a cauliflower WSCP, or could result from Chl or proteins aggregates (Schmidt *et al.*, 2003; Bednarczyk *et al.*, 2015). The conformation changes could also be due to a transition between dimer to tetramer oligomerizations, but such dimers have never been observed experimentally (Palm *et al.*, 2017).

Another explanation of the biphasic binding event could be due to difference of Chl stoichiometry inside the major tetrameric complexes. In WSCP tetramer, each subunit binds a single Chl and the complex is organized into two open sandwich structures, each constituted by a WSCP-Chl dimer (Horigome *et al.*, 2007; Bednarczyk *et al.*, 2016; Agostini *et al.*, 2019). Some studies suggested different Chl stoichiometries inside WSCP-Chl tetrameric complexes (Schmidt *et al.*, 2003; Hughes *et al.*, 2006). Recently, Palm *et al.* (2017) and Agostini *et al.* (2018) showed that at low Chl concentrations, a stable tetramer was formed by binding to only two Chl molecules. Such complexes are as stable as those full of Chl. Moreover, the complexes containing two Chls can scavenge additional Chls to fill the vacant binding sites. We demonstrate herethat the biphasic binding event revealed the presence of two populations of BnD22-Chl complexes, a half Chl state (two Chls) and a fully Chl state (4 Chls). So, the event 1 corresponds to fully pigmented states (4BnD22-4Chl) where the BnD22 is reconstituted with excess of Chl, and the event 2 corresponds to the half-pigmented state (4BnD22-2Chl) where BnD22 was reconstituted with limited Chls (Fig. 6).

4.4. BnD22 shows a strong selectivity to Chla compared to Chlb

Although a preference of Chlb has been shown to LvWSCP (a WSCP IIB), there was no report describing the Chla preference for BoWSCP a WSCP IIA protein. These two WSCPs have respectively 36% and 93.5% similarity to BnD22 (Fig. S4). Girr *et al.* (2020) reported that the Chl selectivity was mainly controlled by the affinities. However, they failed to show any Chl preference to BoWSCP by the Kd values obtained for Chla and Chlb. In this study, the Kd values obtained by MST derived method for BnD22 to Chla were smaller than those of Chlb indicating that BnD22 displays a higher affinity for Chla and supports the idea that Chla/Chlb preference is controlled by Kd values (Girr *et al.*, 2020). The preference of BnD22 for Chla could partly be explained by the presence of PVCNEL motif in its polypeptide sequence (Palm *et al.*, 2018) (Fig. S3). Moreover, it is in agreement with the Chla/Chlb content in native and recombinant WSCP IIA (Murata *et al.*, 1971).

4.5. BnD22 has an effect on Chl photostability

The decrease of Chls photobleaching in presence of BnD22 corroborates the ability of BnD22 to protect the bound Chls against photodynamic damage as previously shown for several WSCPs (Schmidt *et al.*, 2003; Agostini *et al.*, 2017; Palm *et al.*, 2019). This protective role would be due to the packaging of Chls within a well-protected hydrophobic core (Horigome *et al.*, 2007; Agostini *et al.*, 2017; Lemke and Götze, 2019; Palm *et al.*, 2019). In our experimental conditions, highest photoprotection of Chla compared to Chlb in BnD22 complexes might due to a difference in the binding to BnD22 between Chls. Interestingly, in agreement with Palm *et al.* (2017), in our conditions, the Chla and Chlb are also protected against photooxidation in both types of BnD22-Chl complexes at half and fully pigmented states. But, in contrary to Palm *et al.* (2017) that observed, similar photobleaching rates whatever the stoichiometry of Chla inside the WSCP complexes, our results showed a photoprotection of Chla or Chlb better in 4BnD22-2Chls than in 4BnD22-4Chl complexes (Table 2). The difference in results obtained by Palm *et al.* (2017) with ours, could be explained by the time of illumination (one hour versus a few seconds respectively).

5. Conclusion

For the first time, we demonstrate that Chl photobleaching traking by use of a Monoliht equipment is an appropriate method to measure the binding affinities of WSCP to Chla or Chlb where circular dichroism method failed. By this novel method, we have demonstrated that BnD22, a WSCP IIA, is able to bind both Chla and/or Chlb with a Chla preference. Moreover, it appeared that depending on Chl/WSCP ratio, two distinct binding events were identified, each with specific binding affinities (range around nM and µM). This finding is consistent with previous results showing that WSCPs can bind 2 or 4 Chls molecules which could be protected differently from photodamage within WSCP-Chl complexes (Fig. 7). Our results demonstrate the technical feasibility of the method proposed in this study. It has the potential to become a valuable and fast approach for analyzing wild-type as well as mutated WSCPs difference in their affinity and their selectivity to Chls or its precursors or its derivatives. This derived-MST method as a screening tool is very promising and opens new possibilities to characterize assembly process between WSCPs and pigments. Future studies on other WSCP members than BnD22 could be performed to improve our knowledge on WSCP properties and their role in plants. This offers new opportunities to understand the presence of significant number of *WSCPs* genes in *Brassicaceae.*

Data and materials availability statement

All materials and data analyzed in this study are available from the corresponding author.

Funding

This research was supported by national collaborative project entitled RAPSODYN (ANR-11-BTBR-0004) funded by the program "Investments for the Future". This work was also supported by PhD grant to Youssef Bouargalne from the French Research Ministry (MESR, Ministère de l'Enseignement Supérieur et de la Recherche) and by the Brittany regional authority.

Declaration of competing interest

The authors declare that they have no conflict of interest. The funders had no role in study design, data collection and analysis, decision to publish, or preparation of the manuscript.

Acknowledgments

We thank Jean-François Hubert for helpful discussions about recombinant protein production and purification. We thank Katarzyna Walkiewicz and Pierre Soule (NanoTemper) for their suggestions regarding the MST experiment design and for being our NanoTemper contact. We are grateful to the Spectroscopies-DCTP core facility (UMS Biosit, Université de Rennes 1-Campus de Villejean- 35043 RENNES Cedex, FRANCE) for access to their facilities.

Author Contributions

L.C.F. and C.D. acquired financial support, conceived, designed and supervised the research. Y.B. conceived, designed and performed experiments, analyzed data, prepared figures and wrote the original draft. V.C. and A.C, prepared expression plasmids and contributed to protein purification. F.G. performed the protein purification and EMSA experiment. C.R.N. conceived, designed, validated and performed technical guidance for the MST experiments. All authors have read and agreed to the published version of the manuscript.

References

Agostini A, Meneghin E, Gewehr L, Pedron D, Palm DM, Carbonera D, Paulsen H, Jaenicke E, Collini E. **2019**. How water-mediated hydrogen bonds affect chlorophyll a/b selectivity in water soluble chlorophyll protein. *Sci. Rep.* **9**:18255. https://doi.org/10.1038/s41598-019-54520-4

Agostini A, Palm DM, Paulsen H, Carbonera D. **2018**. Optically detected magnetic resonance of chlorophyll triplet states in water soluble chlorophyll proteins from *Lepidium virginicum*: evidence for excitonic interaction among the four pigments. *J. Phys. Chem. B* **122**: 6156-6163. https://doi.org/10.1021/acs.jpcb.8b01906

Agostini A, Palm DM, Schmitt FJ, Albertini M, Valentin M Di, Paulsen H, Carbonera D. **2017**. An unusual role for the phytyl chains in the photoprotection of the chlorophylls bound to water soluble chlorophyll binding proteins. *Sci. Rep.* **7**: 1-13. https://doi.org/10.1038/s41598-017-07874-6.

Annamalai P and Yanagihara S. **1999**. Identification and characterization of a heat-stress induced gene in cabbage encodes a Kunitz type protease inhibitor. *J. Plant Physiol.* **155**: 226-233. https://doi.org/10.1016/S0176-1617(99)80011-X.

Bednarczyk D, Dym O, Prabahar V, Peleg Y, Pike DH, Noy D. **2016**. Fine tuning of chlorophyll spectra by protein-induced ring deformation. *Angewandte Chemie - International Edition* **55**: 6901-6905. https://doi.org/10.1002/anie.201512001.

Bednarczyk D, Takahashi S, Satoh H, Noy D. **2015**. Assembly of water-soluble chlorophyll-binding proteins with native hydrophobic chlorophylls in water-in-oil emulsions. *Biochim. Biophys. Acta.* **1847**: 307-313. https://doi.org/10.1016/j.bbabio.2014.12.003.

Boex-Fontvieille E, Rustgi S, Reinbothe S, Reinbothe C. **2015a**. A Kunitz-type protease inhibitor regulates programmed cell death during fower development in *Arabidopsis thaliana*. *J. Exp. Bot.* **66**: 6119-6135. https://doi.org/10.1093/jxb/erv327.

soluble chlorophyll protein is involved in herbivore resistance activation during greening of *Arabidopsis thaliana*. *Proc. Natl. Acad. Sci. USA* **112**: 7303-7308. https://doi.org/10.1073/pnas.1507714112.

Damaraju S, Schlede S, Eckhardt U, Lokstein H, Grimm B. **2011**. Functions of the water soluble chlorophyll-binding protein in plants. *J. Plant Physiol.* **168**: 1444-1451. https://doi.org/10.1016/j.jplph.2011.02.007.

Desclos M, Dubousset L, Etienne P, Le Cahérec F, Satoh H, Bonnefoy J, Ourry A, Avice J-C. **2008**. A proteomic profiling approach to reveal a novel role of *Brassica napus* Drought 22 kD/ water soluble chlorophyll binding protein in young leaves during nitrogen remobilization induced by stressful conditions. *Plant Physiol.* **147**: 1830-1844. https://doi.org/10.1104/pp.108.116905.

Downing WL, Mauxion F, Fauvarque M -O, Reviron M -P, De Vienne D, Vartanian N, Giraudat J. **1992**. A *Brassica napus* transcript encoding a protein related to the Kunitz protease inhibitor family accumulates upon water stress in leaves, not in seeds. *Plant J.* **2**: 685-693. https:// doi.org/10.1046/j.1365-313X.1992.t01-11-00999.x.

Entzian C and Schubert T. **2016**. Studying small molecule-aptamer interactions using MicroScale Thermophoresis (MST). *Methods* **97**: 27-34. https:// doi.org/10.1016/j.ymeth.2015.08.023.

Girr P, Kilper J, Pohland AC, Paulsen H. **2020**. The pigment binding behaviour of water-soluble chlorophyll protein (WSCP). *Photochem. Photobiol. Sci.***19**: 695-712. https:// doi.org/10.1039/d0pp00043d.

Halls CE, Rogers SW, Oufattole M, Østergard O, Svensson B, Rogers JC. **2006**. A Kunitz-type cysteine protease inhibitor from cauliflower and Arabidopsis. *Plant Sci.* **170**: 1102-1110. https://doi.org/10.1016/j.plantsci.2006.01.018

Horigome D, Satoh H, Itoh N, Mitsunaga K, Oonishi I, Nakagawa A, Uchida A. **2007**. Structural mechanism and photoprotective function of water-soluble chlorophyll-binding protein. *J. Biol. Chem.* **282**: 6525-6531. https://doi.org/10.1074/jbc.M609458200.

Hughes JL, Razeghifard R, Logue M, Oakley A, Wydrzynski T, Krausz E. **2006**. Magneto-optic spectroscopy of a protein tetramer binding two exciton-coupled chlorophylls. *J. Am. Chem. Soc.* **128**: 3649-3658. https://doi.org/10.1021/ja056576b.

Ilami G, Nespoulous C, Huet JC, Vartanian N, Pernollet JC. **1997**. Characterization of BnD22, a drought-induced protein expressed in *Brassica napus* leaves. *Phytochem.* **45**: 1-8. https://doi.org/10.1016/S0031-9422(96)00788-1.

Jerabek-Willemsen M, André T, Wanner R, Roth HM, Duhr S, Baaske P, Breitsprecher D. **2014**. MicroScale Thermophoresis: Interaction analysis and beyond. *J. Mol. Str*. **1077**: 101-113. https://doi.org/10.1016/j.molstruc.2014.03.009.

Laemmli UK. **1970**. Cleavage of structural proteins during the assembly of the head of bacteriophage T4. *Nature* **227**: 680-685. https://doi.org/10.1038/227680a0.

Lemke O and Götze JP. **2019**. On the stability of the water soluble chlorophyll binding protein (WSCP) studied by molecular dynamics simulations. *J. Phys. Chem.* B **123**:10594-10604. https://doi.org/10.1021/acs.jpcb.9b07915.

Murata T, Toda F, Uchino K, Yakushiji E 1971. Water soluble chlorophyll protein of *Brassica oleracea* var. botrys (cauliflower). *Biochim. Biophys. Acta* **245**: 208-215. https://doi.org/10.1016/0005-2728(71)90023-5.

Mork-Jansson AE and Eichacker LA. **2018**. Characterization of chlorophyll binding to LIL3. *PLoS ONE* **13**: 1-14. https://doi.org/10.1371/journal.pone.0192228.

Mork-Jansson AE and Eichacker LA. **2019**. A strategy to characterize chlorophyll protein interaction in LIL3. *Plant Methods* **15**: 1-13. https://doi.org/10.1186/s13007-018-0385-5

Nakano RT, Yamada K, Bednarek P, Nishimura M, Hara-Nishimura I. **2014**. ER bodies in plants of the Brassicales order: biogenesis and association with innate immunity. *Front. Plant Sci.* **5**: 1-17. https://doi.org/10.3389/fpls.2014.00073.

Palm DM, Agostini A, Averesch V, Girr P, Werwie M, Takahashi S, Satoh H, Jaenicke E, Paulsen H. **2018**. Chlorophyll a/b binding-specificity in water soluble chlorophyll protein. *Nat. Plants* **4**: 920-929. https://doi.org/10.1038/s41477-018-0273-z.

Palm DM, Agostini A, Pohland AC, Werwie M, Jaenicke E, Paulsen H. **2019**. Stability of water woluble chlorophyll protein (WSCP) depends on phytyl conformation. *ACS Omega* **4**: 7971-7979. https://doi.org/10.1021/acsomega.9b00054.

Palm DM, Agostini A, Tenzer S, Gloeckle BM, Werwie M, Carbonera D, Paulsen H. **2017**. Water soluble chlorophyll protein (WSCP) stably binds two or four chlorophylls. *Biochem.* **56**: 1726-1736. https://doi.org/10.1021/acs.biochem.7b00075.

Prabahar V, Afriat-Jurnou L, Paluy I, Peleg Y, Noy D. **2020**. New homologues of Brassicaceae water-soluble chlorophyll proteins shed light on chlorophyll binding, spectral tuning, and molecular evolution. *FEBS J.* **287**: 991-1004. https://doi.org/10.1111/febs.15068.

Renger G, Pieper J, Theiss C, Trostmann I, Paulsen H, Renger T, Eichler HJ, Schmitt FJ. 2011. Water soluble chlorophyll binding protein of higher plants: a most suitable model system for basic analyses of pigment–pigment and pigment–protein interactions in chlorophyll protein complexes. *J. of Plant Physiol.*, **168**, 1462-1472. https://doi.org/10.1016/j.jplph.2010.12.005

Reviron M-P, Vartanian N, Sallantin M, Huet J-C, Pernollet J-C, de Vienne D. **1992**. Characterization of a novel protein induced by progressive or rapid drought and salinity in *Brassica napus* leaves. *Plant Physiol.* **100**: 1486-1493. https://doi.org/10.1104/pp.100.3.1486.

Rustgi S, Boex-Fontvieille E, Reinbothe C, von Wettstein D, Reinbothe S. **2017**. Serpin1 and WSCP differentially regulate the activity of the cysteine protease RD21 during plant development in *Arabidopsis thaliana*. *Proc. Natl. Acad. Sci. USA* **114**: 2212-2217.

https://doi.org/10.1073/pnas.1621496114.
Satoh H, Nakayama K, Okada M. **1998**. Molecular cloning and functional expression of a water soluble chlorophyll protein, a putative carrier of chlorophyll molecules in cauliflower. *J. Biol. Chem.* **273**: 30568-30575. https://doi.org/10.1074/jbc.273.46.30568.
Satoh H, Uchida A, Nakayama K, Okada M. **2001**. Water soluble chlorophyll protein in Brassicaceae plants is a stress-induced chlorophyll-binding protein. *Plant Cell Physiol*. **42**: 906-911. https://doi.org/10.1093/pcp/pce117
Schmidt K, Fufezan C, Krieger-Liszkay A, Satoh H, Paulsen H. **2003**. Recombinant water soluble chlorophyll protein from *Brassica oleracea* var. botrys binds various chlorophyll derivatives. *Biochem.***42**: 7427-7433. https://doi.org/10.1021/bi034207r.
Takahashi S, Yanai H, Nakamaru Y, Uchida A, Nakayama K, Satoh H. **2012**. Molecular cloning, characterization and analysis of the intracellular localization of a water soluble chlorophyll binding protein from brussels sprouts (*Brassica oleracea* var. gemmifera). *Plant Cell Physiol.* **53**: 879-891. https://doi.org/10.1093/pcp/pcs031.
Takahashi S, Ono M, Uchida A, Nakayama K, Satoh H. **2013a**. Molecular cloning and functional expression of a water soluble chlorophyll binding protein from Japanese wild radish. *J. Plant Physiol.* **170**: 406-412. https://doi.org/10.1016/j.jplph.2012.10.007.
Takahashi S, Yanai H, Oka-Takayama Y, Zanma-Sohtome A, Fujiyama K, Uchida A, Nakayama K, Satoh H. **2013b**. Molecular cloning, characterization and analysis of the intracellular localization of a water soluble chlorophyll- binding protein (WSCP) from Virginia pepperweed (*Lepidium virginicum*), a unique WSCP that preferentially binds chlorophyll b *in vitro*. *Planta* **238**: 1065-1080. https://doi.org/1065–1080. 10.1007/s00425-013-1952-7.
Takahashi S, Uchida A, Nakayama K, Satoh H. **2014**. The C-terminal extension peptide of non-photoconvertible water- oluble chlorophyll binding proteins (Class II WSCPs) affects their solubility and stability: comparative analyses of the biochemical and chlorophyll-binding properties of recombinant *Brassica*, *Raphanus* and *Lepidium* WSCPs with or without their C-terminal extension peptides. *Protein J.* **33**: 75-84. https://doi.org/10.1007/s10930-013-9539-5
Theiss C, Trostmann I, Andree S, Schmitt FJ, Renger T, Eichler HJ, Paulsen H, Renger G. **2007**. Pigment - pigment and pigment - protein interactions in recombinant water soluble chlorophyll proteins (WSCP) from cauliflower. *J. Phys. Chem. B* **111**: 13325-13335. https://doi.org/10.1021/jp0723968.
Wienken CJ, Baaske P, Rothbauer U, Braun D, Duhr S. **2010**. Protein-binding assays in biological liquids using microscale thermophoresis. *Nat. Commun.* **1**. https://doi.org/10.1038/ncomms1093.

Figures

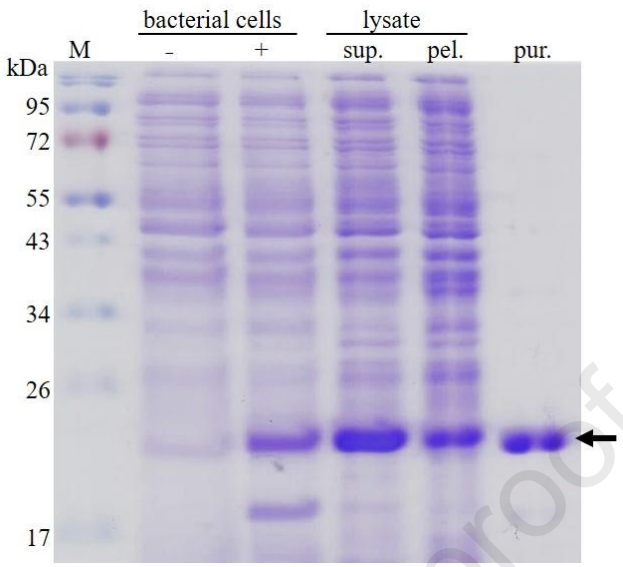

Fig. 1. Subcellular fractionation and purification of BnD22 expressed in *E. coli*

Proteins from cell extracts of uninduced *E. coli* (-) or after IPTG-induced BnD22 expression (+), from supernatant (sup.) or pellet (pel.) protein fractions of sonicated *E. coli*, and purified protein using Ni^{2+} affinity chromatography (pur.) were separated by 15% SDS–PAGE and stained with Coomassie Blue. The protein markers are indicated as M. Black arrow indicates the position BnD22.

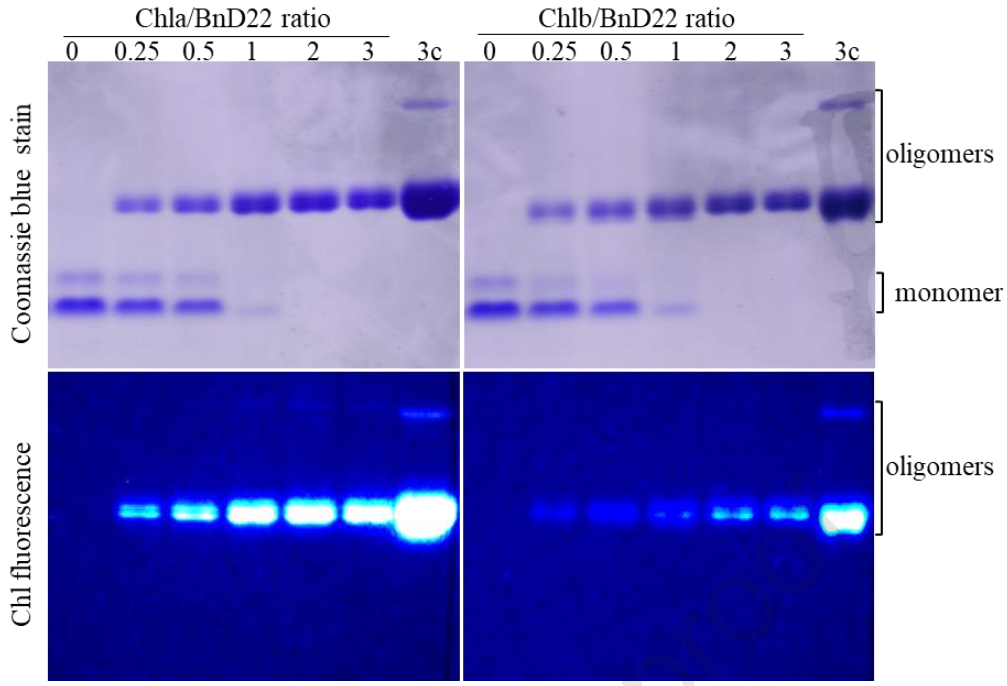

Fig. 2. Conformational changes monitoring of BnD22 upon binding to Chla (left) or Chlb (right).

20 µM of purified BnD22 were mixed with 0, 5, 10, 15, 20, 40, 60 µM of Chla or Chlb (0, 0.25, 0.5, 0.1, 1, 2 or 3 Chls/protein ratio) in binding buffer (50 mM Tris-HCl (pH 7.5), 150 mM NaCl, 0.04% NP40). After 30 min of binding, BnD22-Chls were visualized by electrophoretic mobility on 12% native PAGE stained with Coomassie blue (upper panel) or by detection of Chl fluorescence (lower panel). To visualize the high molecular mass oligomer, the complexes obtained at the Chl/BnD22=3 condition were concentrated (3c).

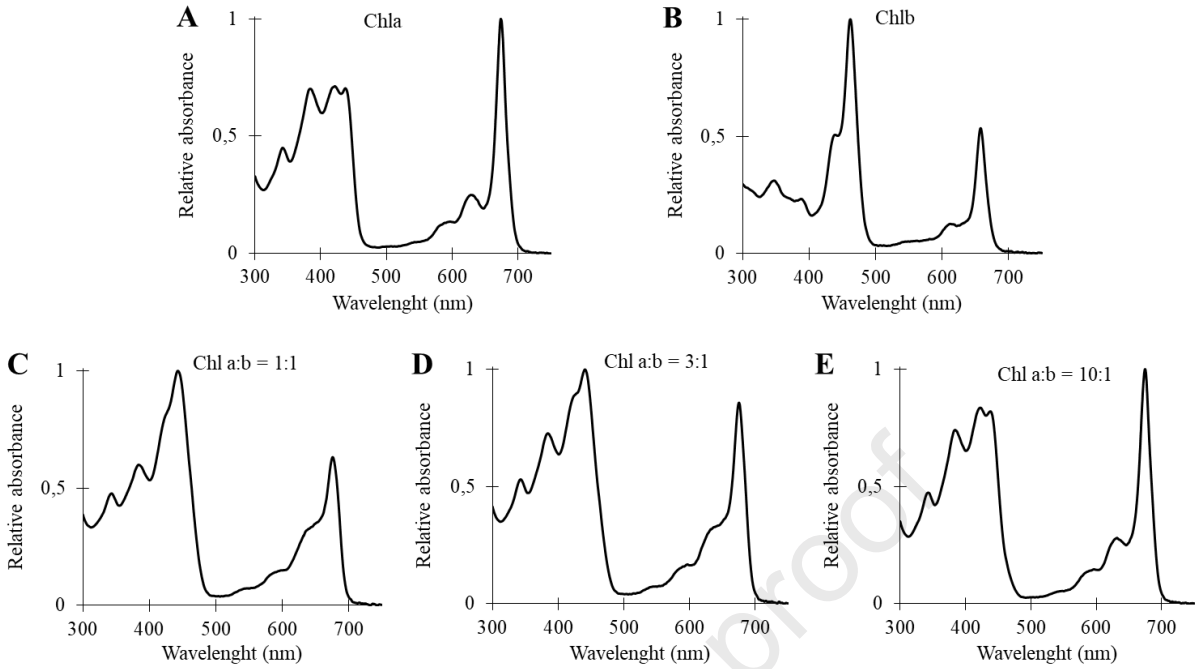

Fig. 3. UV-visible absorption spectra of reconstituted BnD22 with Chls.

20 µM of purified BnD22 were mixed with 60 µM of Chla (A), Chlb (B), or three different Chla/b mixtures : 1/1 (C), 3/1 (D), 10/1 (E) ratio in binding buffer (50 mM Tris-HCl (pH 7.5), 150 mM NaCl, 0.04% NP40). After EMSA, the BnD22-Chl complexes were eluted from gels and their UV-visible absorption spectra were performed between 300 and 750 nm.

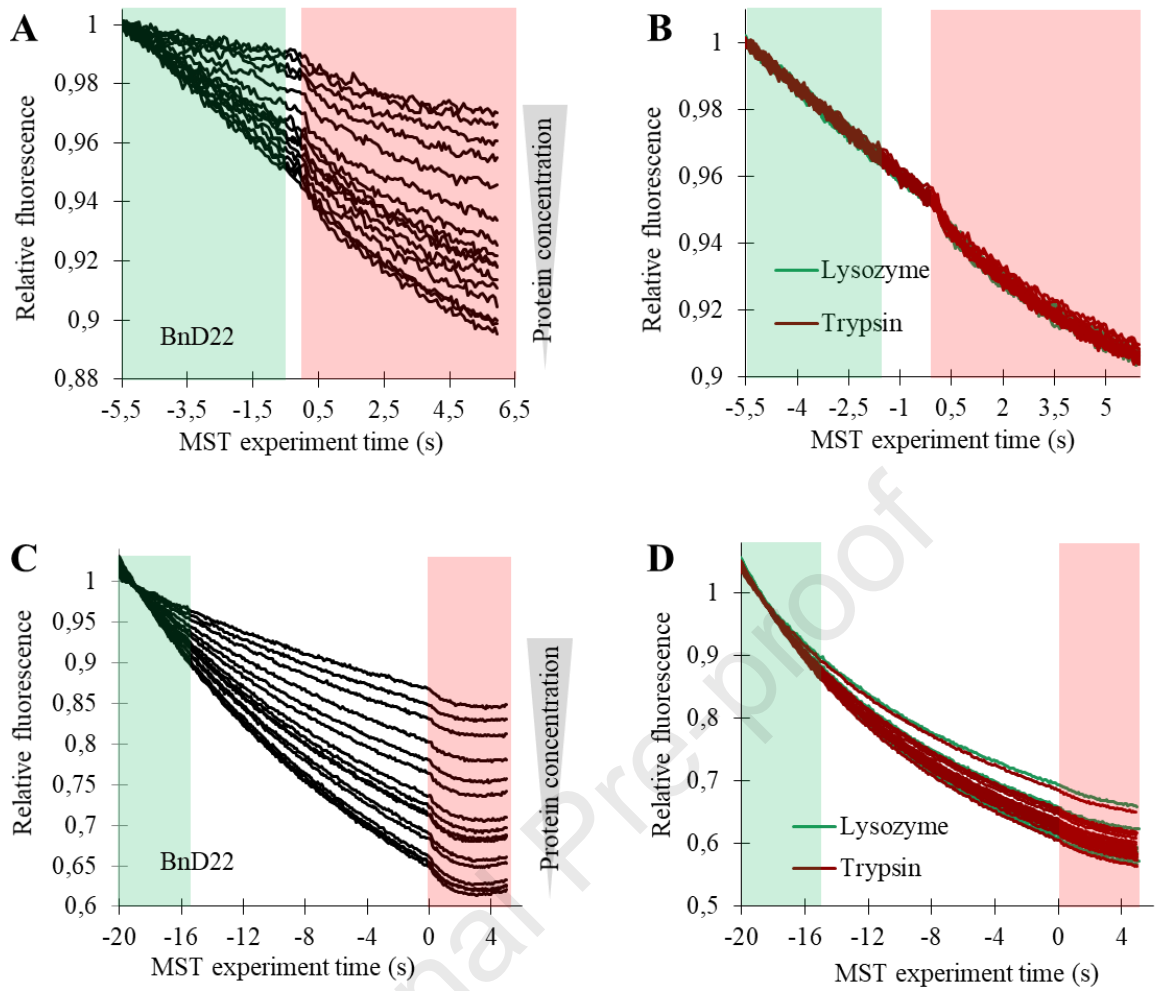

Fig. 4. Unprocessed MST traces of Chla (A, B) or Chlb (C, D) binding to BnD22 (A, C) or lysozyme or trypsin (B, D).

Constant concentrations of Chla (50 nM) or Chlb (80 nM) were mixed with a titration series of BnD22 or non-relevant proteins (trypsin or lysozyme) used as negative controls in binding buffer (50 mM Tris-HCl (pH 7.5), 150 mM NaCl, 0.04% NP40). The protein concentrations used varied from 80 to 0.124 µM. After 30 min of binding, MST experiments were performed at 100 % LED and 40 % MST power. Red area defines MST IR laser application. Data from the green highlighted region (the first 5 s of excitation) were used to calculate the bleaching rates.

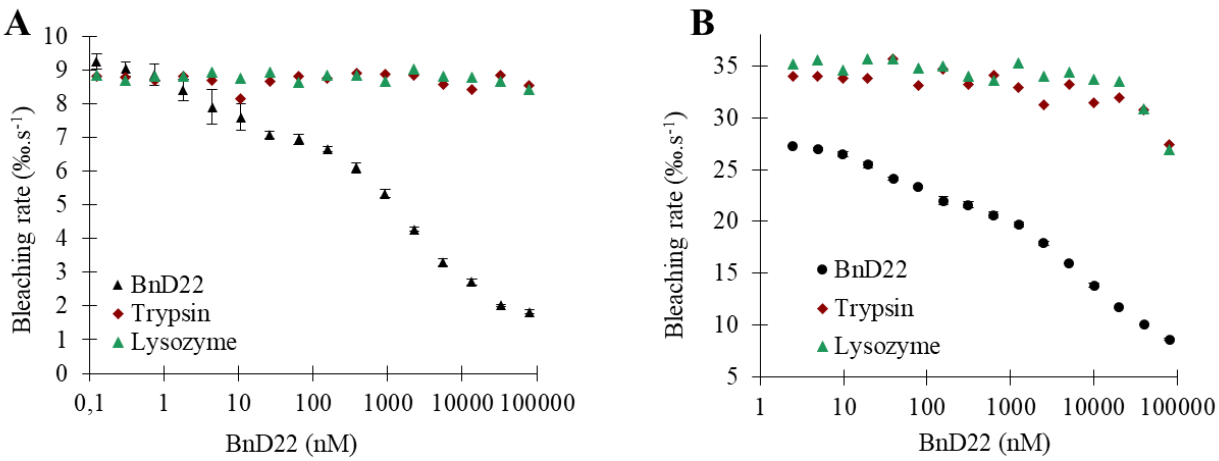

Fig. 5. Bleaching rates of Chla (A) or Chlb (B) in presence of BnD22 or negative controls (lysozyme and trypsin).

Constant concentrations of Chla (50 nM) or Chlb (80 nM) were mixed with a titration series of BnD22 or negative controls (trypsin or lysozyme) in binding buffer (50 mM Tris-HCl (pH 7.5), 150 mM NaCl, 0.04% NP40). After 30 min of binding, MST experiments were performed at 100 % LED and 40 % MST power. The bleaching rates, calculated in the first 5 s of excitation, were plotted against protein concentrations.

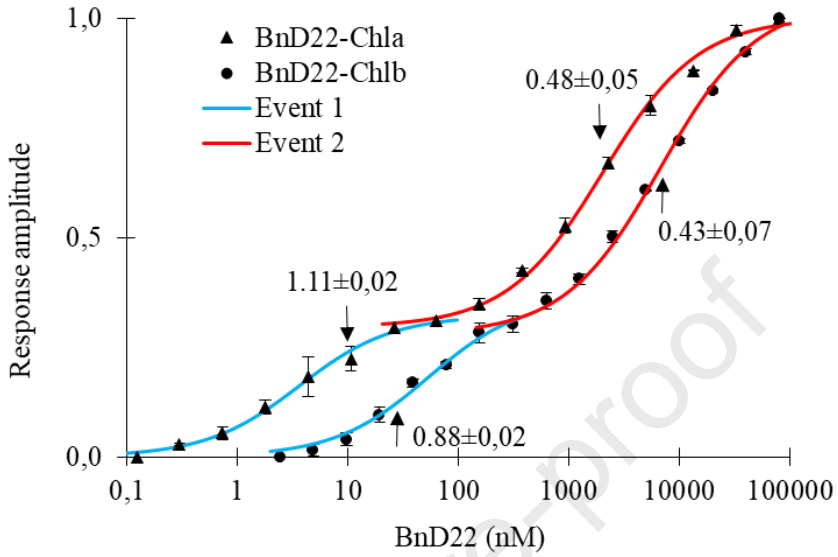

Fig. 6. Biphasic interaction between BnD22 and Chla or Chlb.

Constant concentrations of Chla (50 nM) or Chlb (80 nM) were mixed with a titration series of BnD22 in binding buffer (50 mM Tris-HCl (pH 7.5), 150 mM NaCl, 0.04% NP40). After 30 min of binding, MST experiments were performed at 100 % LED and 40 % MST power. Response amplitude was calculated from the bleaching rates and plotted against BnD22 concentrations. Each binding event was fitted individually to define binding parameters (summarized in Table 3). Each value represents the mean ± SD (n=3). For two binding conditions at 5-fold Chl molar excess (event 1) and 40-fold BnD22 molar excess (event 2), the molar Chl/protein ratio inside BnD22 complexes are indicated by arrows and were determined from absorption spectra of purified BnD22-Chla or BnD22-Chlb complexes (according to Palm *et al.*, 2017).

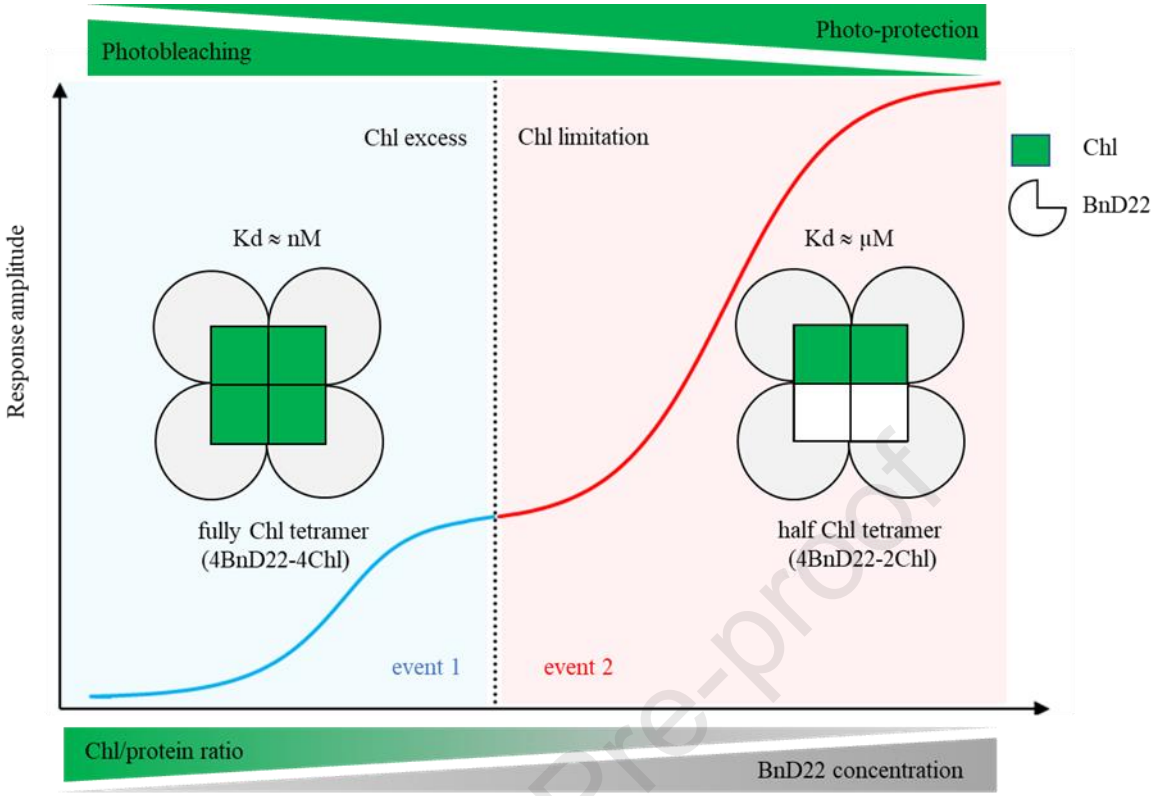

Fig. 7. Model of biphasic BnD22-Chls interactions.

The biphasic binding event resulted from two populations of BnD22-Chl tetrameric complexes, fully (4 Chl by tetramer, 4BnD22-4Chl) and a half (2 Chl by tetramer, 4BnD22-2Chl) Chl states, which depended on Chl/WSCP ratio in the binding condition. The Chls were positioned in the 2ChlaWSCP complex according to Palm *et al.*, (2017), with one dimer binding a tightly coupled Chl pair and the other dimer with two empty binding sites. Binding affinities between Chl and BnD22 were more important during the formation of 4BnD22-2Chl complexes compare to fully Chl state (4BnD22-4Chl). Greater photoprotection of Chl inside the 4BnD22-2Chl complexes was observed.

Dotted line indicates the equimolar Chl/protein ratio (=1). The blue and red highlighted regions indicate the Chl excess (Chl/protein ratio >1) and Chl limitation (Chl/protein ratio <1) respectively.

Tables

Table 1. Effect of binding buffers on initial fluorescence and bleaching rate of Chla and Chlb. 50 nM of Chla or 80 nM of Chlb were added to different buffers and filled into standard MST capillaries. Experiments were performed at 100 % LED. Initial fluorescence (IF) was measured and the bleaching rate (BR) calculated in the first 5 s of excitation. Asterisks indicate significant effect of buffer or detergent for each variable in Kruskal-Wallis test (*P ≤ 0.05; **P ≤ 0.01; NS = not significant).

		initial fluorescence (counts)		bleaching rate (‰.s^{-1})		IF/BR ratio (%)	
buffer	detergent	Chla	Chlb	Chla	Chlb	Chla	Chlb
Tris-HCl 50 mM, pH 7.5 150 mM NaCl	0.59 mM NP40	261±2.8	219±7.8	8.9±0.2	28.0±0.5	29.4±0.3	7.8±0.1
	5.87 mM DDM	241±3.8	165±16.0	8.4±0.7	25.1±0.3	29.0±3.0	6.6±0.6
	34.2 mM OG	293±28.2	207±12.1	11.8±0.1	28.8±0.5	24.9±2.6	7.2±0.3
	3.33 mM IGEPAL	242±6.3	184±11.0	9.4±0.1	28.4±0.8	25.6±0.5	6.5±0.6
sodium phosphate 50 mM, pH 7.5 150 mM NaCl	0.59 mM NP40	262±1.9	214±26.9	9.4±0.3	28.9±4.1	28.0±0.6	7.5±2.0
	5.87 mM DDM	243±5.5	176±23.5	8.4±0.1	29.3±2.0	29.0±0.7	6.0±1.2
	34.2 mM OG	251±4.0	240± 0.4	11.2±0.3	29.4±3.5	22.4±0.2	8.2±1.0
	3.33 mM IGEPAL	234±7.2	173±16.6	9.1±0.1	32.2±2.5	25.6±0.6	5.4±0.9
	buffer	NS	NS	NS	NS	NS	NS
	detergent	**	**	**	NS	**	*

Table 2. Effect of BnD22 on Chls photostability over excitation time.

50 nM of Chla or 80 nM of Chlb were mixed with titration series of BnD22 in binding buffer (50 mM Tris-HCl (pH 7.5), 150 mM NaCl, 0.04% NP40). After 30 min of binding, MST experiments were performed at 100 % LED and 40 % MST power. The bleaching rates (BR) were calculated in the first 5 s of excitation. Levels of photoprotection were determined by the difference between the highest and the lowest BR related to the highest BR. Data are expressed as the mean ± SD (n = 3). Asterisks indicate significant differences between chlorophylls for each variable in the Student's t test (*** $P \leq 0.001$).

	photoprotection (%)		
	overall	event 1	event 2
BnD22-Chla	80.3 ± 0.3	33.2 ± 0.5	74.3 ± 0.6
BnD22-Chlb	68.4 ± 0.8	21.8 ± 2.3	61.4 ± 1.0
	***	***	***

Table 3. Binding parameters of the interaction between BnD22 and Chls.

50 nM of Chla or 80 nM of Chlb were mixed with a titration series of BnD22 in binding buffer containing 50 mM Tris-HCl (pH 7.5), 150 mM NaCl, 0.04% NP40). After 30 min of binding, MST experiments were performed at 100 % LED and 40 % MST power. Response amplitude calculated from the bleaching rates were plotted against BnD22 concentrations (Fig.6). Kd, EC50 and nHill values were calculated for each binding event. Each value represents the mean ± SD (n=3). Asterisks indicate significant differences between chlorophylls for each variable in the Student's t test (**P ≤ 0.01; ***P ≤ 0.001; NS = not significant).

	Kd		EC50		nHill	
	event 1 (nM)	event 2 (µM)	event 1 (nM)	event 2 (µM)	event 1	event 2
BnD22-Chla	3.9±2.2	2.0±0.2	4.5±3.2	2.1±0.3	0.9±0.2	0.8±0.1
BnD22-Chlb	51.4±8.6	6.7±0.7	35.1±9.8	8.1±0.7	1.1±0.2	0.8±0.1
	***	***	**	***	NS	NS

Supplementary data

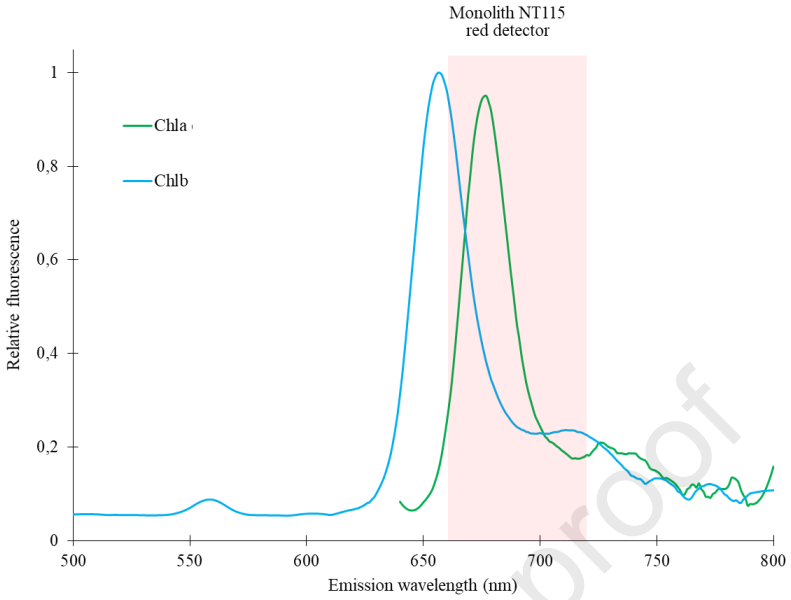

Fig. S1. Chla or Chlb fluorescence emission spectra after excitation at 470 nm and 625 nm. Chla or Chlb were solubilized in binding buffer (50 mM Tris-HCl (pH 7.5), 150 mM NaCl, 0.04 % NP40) and fluorescence spectra were measured on a FluoroMax-2 instrument using two excitation wavelengths 470 nm (for Chlb) and 625 nm (for Chla).

The emission wavelengths of the Monolith NT.115 red fluorescence detector are highlighted in red.

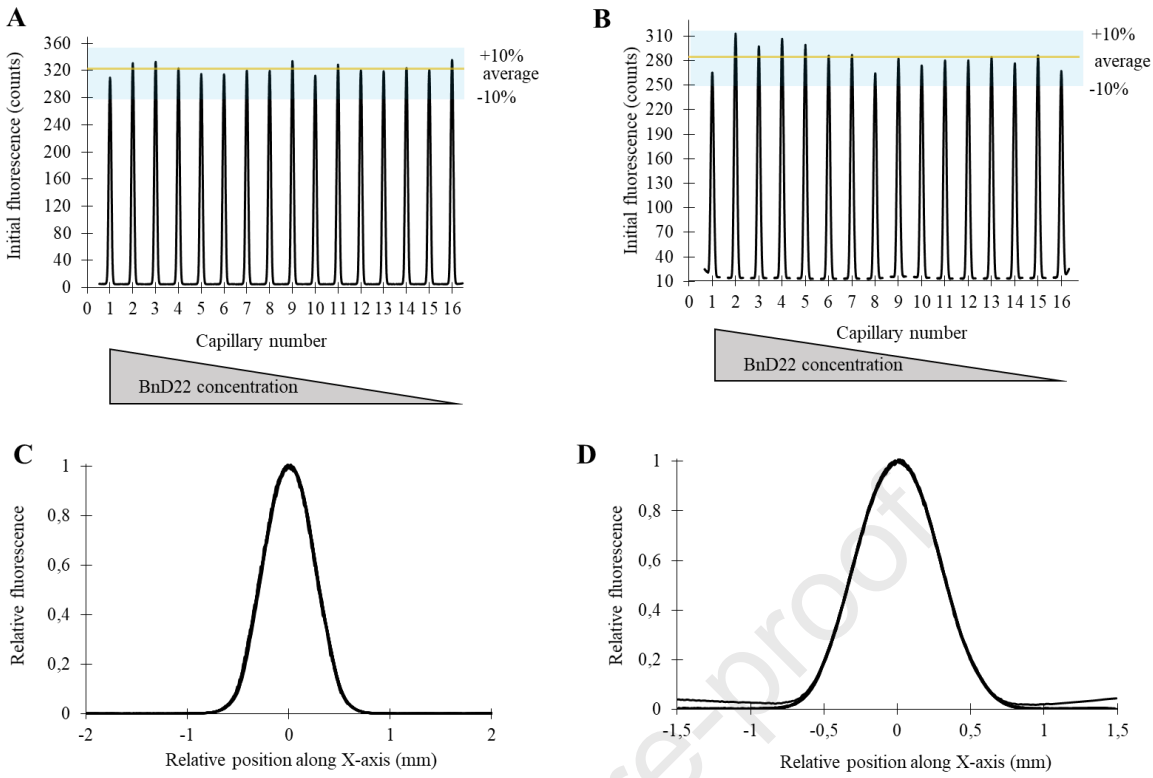

Fig. S2. Data inspection of MST binding experiments between BnD22 and Chla (left) or Chlb (right).

50 nM of Chla or 80 nM of Chlb were mixed with a titration series of BnD22 in binding buffer (50 mM Tris-HCl (pH 7.5), 150 mM NaCl, 0.04% NP40). After 30 min of binding, fluorescence was measured at 100 % LED. Distribution of initial fluorescence was represented either individually for each capillary for Chla (A) or Chlb (B), or normalized and overlayed for Chla (C) or Chlb (D). The variation within ±10 % of the average is highlighted in blue.

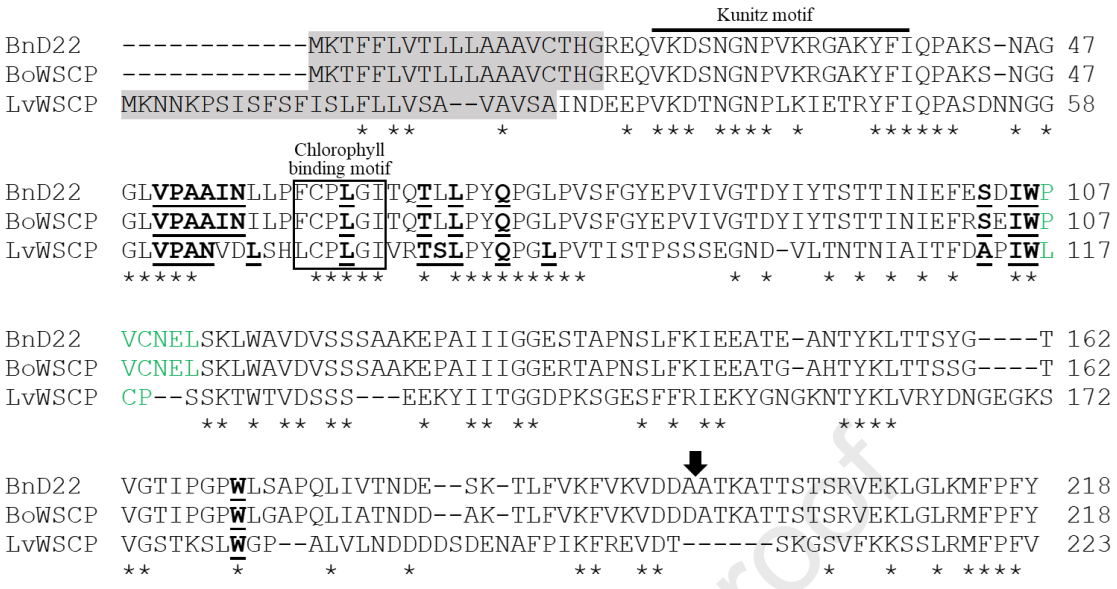

Fig. S3. Sequence alignment of WSCPs from *Brassica napus* (BnD22, uniProt: Q43395), *Brassica oleracea* (BoWSCP, uniProt: Q7GDB3) and *Lepidium virginicum* (LvWSCP, uniProt: O04797).

The signal peptides are shown with a grey background. Black bar indicates the Kunitz motif. The box indicates the region homologous to the chlorophyll binding motif. Chla/b affinity motifs are in green. Amino acids close to the Chls chlorine macrocycle are underlined and bold. Black arrow indicates post-translational cleavage site. The asterisks indicate fully conserved residues.

Information Legends

Figures

Fig. 1. Subcellular fractionation and purification of BnD22 expressed in *E. coli*

Proteins from cell extracts of uninduced *E. coli* (-) or after IPTG-induced BnD22 expression (+), from supernatant (sup.) or pellet (pel.) protein fractions of sonicated *E. coli,* and purified protein using Ni^{2+} affinity chromatography (pur.) were separated by 15% SDS–PAGE and stained with Coomassie Blue. The protein markers are indicated as M. Black arrow indicates the position BnD22.

Fig. 2. Conformational changes monitoring of BnD22 upon binding to Chla (left) or Chlb (right).

20 µM of purified BnD22 were mixed with 0, 5, 10, 15, 20, 40, 60 µM of Chla or Chlb (0, 0.25, 0.5, 0.1, 1, 2 or 3 Chls/protein ratio) in binding buffer (50 mM Tris-HCl (pH 7.5), 150 mM NaCl, 0.04% NP40). After 30 min of binding, BnD22-Chls were visualized by electrophoretic mobility on 12% native PAGE stained with Coomassie blue (upper panel) or by detection of Chl fluorescence (lower panel). To visualize the high molecular mass oligomer, the complexes obtained at the Chl/BnD22=3 condition were concentrated (3c).

Fig. 3. UV-visible absorption spectra of reconstituted BnD22 with Chls.

20 µM of purified BnD22 were mixed with 60 µM of Chla (A), Chlb (B), or three different Chla/b mixtures : 1/1 (C), 3/1 (D), 10/1 (E) ratio in binding buffer (50 mM Tris-HCl (pH 7.5), 150 mM NaCl, 0.04% NP40). After EMSA, the BnD22-Chl complexes were eluted from gels and their UV-visible absorption spectra were performed between 300 and 750 nm.

Fig. 4. Unprocessed MST traces of Chla (A, B) or Chlb (C, D) binding to BnD22 (A, C) or lysozyme or trypsin (B, D).

Constant concentrations of Chla (50 nM) or Chlb (80 nM) were mixed with a titration series of BnD22 or non-relevant proteins (trypsin or lysozyme) used as negative controls in binding buffer (50 mM Tris-HCl (pH 7.5), 150 mM NaCl, 0.04% NP40). The protein concentrations used varied from 80 to 0.124 µM. After 30 min of binding, MST experiments were performed at 100 % LED and 40 % MST power. Red area defines MST IR laser application. Data from the green highlighted region (the first 5 s of excitation) were used to calculate the bleaching rates.

Fig. 5. Bleaching rates of Chla (A) or Chlb (B) in presence of BnD22 or negative controls (lysozyme and trypsin).

Constant concentrations of Chla (50 nM) or Chlb (80 nM) were mixed with a titration series of BnD22 or negative controls (trypsin or lysozyme) in binding buffer (50 mM Tris-HCl (pH 7.5), 150 mM NaCl, 0.04% NP40). After 30 min of binding, MST experiments were performed at 100 % LED and 40 % MST power. The bleaching rates, calculated in the first 5 s of excitation, were plotted against protein concentrations.

Fig. 6. Biphasic interaction between BnD22 and Chla or Chlb.

Constant concentrations of Chla (50 nM) or Chlb (80 nM) were mixed with a titration series of BnD22 in binding buffer (50 mM Tris-HCl (pH 7.5), 150 mM NaCl, 0.04% NP40). After 30 min of binding, MST experiments were performed at 100 % LED and 40 % MST power. Response amplitude was calculated from the bleaching rates and plotted against BnD22 concentrations. Each binding event was fitted individually to define binding parameters (summarized in Table 3). Each value represents the mean ± SD (n=3). For two binding conditions at 5-fold Chl molar excess (event 1) and 40-fold BnD22 molar excess (event 2), the molar Chl/protein ratio inside BnD22 complexes are indicated by arrows and were determined from absorption spectra of purified BnD22-Chla or BnD22-Chlb complexes (according to Palm *et al.*, 2017).

Fig. 7. Model of biphasic BnD22-Chls interactions.

The biphasic binding event resulted from two populations of BnD22-Chl tetrameric complexes, fully (4 Chl by tetramer, 4BnD22-4Chl) and a half (2 Chl by tetramer, 4BnD22-2Chl) Chl states, which depended on Chl/WSCP ratio in the binding condition. The Chls were positioned in the 2ChlaWSCP complex according to Palm *et al.* (2017), with one dimer binding a tightly coupled Chl pair and the other dimer with two empty binding sites. Binding affinities between Chl and BnD22 were more important during the formation of 4BnD22-2Chl complexes compare to fully Chl state (4BnD22-4Chl). Greater photoprotection of Chl inside the 4BnD22-2Chl complexes was observed.

Dotted line indicates the equimolar Chl/protein ratio (=1). The blue and red highlighted regions indicate the Chl excess (Chl/protein ratio >1) and Chl limitation (Chl/protein ratio <1) respectively.

Tables

Table 1. Effect of binding buffers on initial fluorescence and bleaching rate of Chla and Chlb. 50 nM of Chla or 80 nM of Chlb were added to different buffers and filled into standard MST capillaries. Experiments were performed at 100 % LED. Initial fluorescence (IF) was measured and the bleaching rate (BR) calculated in the first 5 s of excitation. Asterisks indicate significant effect of buffer or detergent for each variable in Kruskal-Wallis test (*P ≤ 0.05; **P ≤ 0.01; NS = not significant).

Table 2. Effect of BnD22 on Chls photostability over excitation time.
50 nM of Chla or 80 nM of Chlb were mixed with titration series of BnD22 in binding buffer (50 mM Tris-HCl (pH 7.5), 150 mM NaCl, 0.04% NP40). After 30 min of binding, MST experiments were performed at 100 % LED and 40 % MST power. The bleaching rates (BR) were calculated in the first 5 s of excitation. Levels of photoprotection were determined by the difference between the highest and the lowest BR related to the highest BR. Data are expressed as the mean ± SD (n = 3). Asterisks indicate significant differences between chlorophylls for each variable in the Student's t test (*** P ≤ 0.001).

Table 3. Binding parameters of the interaction between BnD22 and Chls.
50 nM of Chla or 80 nM of Chlb were mixed with a titration series of BnD22 in binding buffer containing 50 mM Tris-HCl (pH 7.5), 150 mM NaCl, 0.04% NP40). After 30 min of binding, MST experiments were performed at 100 % LED and 40 % MST power. Response amplitude calculated from the bleaching rates were plotted against BnD22 concentrations (Fig.6). Kd, EC50 and nHill values were calculated for each binding event. Each value represents the mean ± SD (n=3). Asterisks indicate significant differences between chlorophylls for each variable in the Student's t test (**P ≤ 0.01; ***P ≤ 0.001; NS = not significant).

Highlights

Photobleaching is a sensitive method to measure the Chl binding affinities of WSCPs.

BnD22, a WSCP IIA, shows stronger Chl affinity and selectivity for Chla than Chlb.

BnD22 presents different affinities for Chls according to Chl/protein ratio.

Two forms of oligomeric complexes lead to biphasic process of BnD22-Chls binding.

Level of Chl photoprotection is according to the oligomeric complexes forms.

Declaration of interests

☒ The authors declare that they have no known competing financial interests or personal relationships that could have appeared to influence the work reported in this paper.

☐ The authors declare the following financial interests/personal relationships which may be considered as potential competing interests: